Dispersion Engineering for Vertical Microcavities Using Subwavelength Gratings

Zhaorong Wang, Bo Zhang, and Hui Deng*
Department of Physics, University of Michigan, Ann Arbor, Michigan 48109-1040, USA
(Received 23 September 2014; published 17 February 2015)

We show that the energy-momentum dispersion of a vertical semiconductor microcavity can be modified by design using a high-index-contrast subwavelength grating (SWG) as a cavity mirror. We analyze the angular dependence of the reflection phase of the SWG to illustrate the principles of dispersion engineering. We show examples of engineered dispersions such as ones with much reduced or increased energy density of states and one with a double-well-shaped dispersion. This method of dispersion engineering is compatible with maintaining a high cavity quality factor and incorporating fully protected active media inside the cavity, thus enabling the creation of new types of cavity quantum electrodynamics systems.

DOI: 10.1103/PhysRevLett.114.073601 PACS numbers: 42.50.Pq, 42.50.Nn, 42.55.Sa, 42.79.Dj

The energy-momentum dispersion is a fundamental property of a photonic system. The capability to modify the dispersion using engineered photonic systems is at the heart of modern photonic technologies and the cavity quantum electrodynamics research. For example, dispersion determines the phase and group velocities and, thus, the propagation of the electromagnetic modes [1]. Dispersion also controls the density of states (DOS) of the photonic modes, and, thus the matter-light interactions in the system [2]. Recently, dispersion engineering has been used in many-body atomic systems to create synthetic magnetic fields [3], enabling the simulation of quantum orders in non-Abelian gauge fields. It was also proposed as a method to create exotic quantum orders in many-body photonic or matter systems [4].

Dispersion engineering has been realized using engineered photonic structures including metamaterials [5–8] and photonic crystals (PhCs) [9–11]. However, metamaterials containing metal constituents suffer from intrinsic Ohmic losses; 2D photonic crystals have large radiation losses for the modes in the light cone. In addition, due to the large surface-to-volume ratio of metamaterials and PhCs, active media embedded inside are prone to surface recombination. These effects limit their usage in applications requiring minimal loss or spatially extended matter-light coupling.

In this Letter, we demonstrate a new method to engineer the dispersions of all-dielectric 1D or 2D vertical microcavities, compatible with lossless embedment of active media. We revisit the century-old resonance condition of a Fabry-Perot cavity and demonstrate dispersion engineering by designing the angular dependence of the reflection phase of a nonconventional cavity mirror. We show that strong angular dependence of the reflection phase of a subwavelength grating (SWG) can be achieved due to the unique symmetry properties of SWGs. As a result, photonic and polaritonic dispersions can be created with curvatures differing by many orders of magnitude. Flat or double-well-shaped dispersions can also be created. Our method of dispersion engineering enables greater flexibility in controlling the photonic modes and matter-light interactions in widely used quantum-well and quantum-dot microcavities. It may allow, for example, the change of the group velocity of the mode, enhanced Purcell effect without additional transverse confinement, and optimized carrier dynamics for polariton lasers with lower threshold. It may open a door to the creation of many-body polariton systems with unusual dispersions and quantum orders [12].

The energy vs in-plane momentum dispersion of a Fabry-Perot-type cavity is governed by the angular dependence of the reflection phase of the cavity mirrors. This is shown by the round-trip phase condition for the cavity resonance,

$$\phi_1(\omega, k_\parallel) + \phi_2(\omega, k_\parallel) - 2k_{c\perp}d = 2m\pi. \tag{1}$$

Here ω is the angular frequency of the resonance, $k_\parallel$ and $k_{c\perp}$ are the in-plane and longitudinal wave numbers in the cavity layer, respectively, d is the distance between the two cavity mirrors, and m is an integer. The first two terms ϕ_1 and ϕ_2 are the reflection phases of the two cavity mirrors. Equation (1) uniquely determines the dispersion relation $\omega(k_\parallel)$.

Conventional microcavities use mirrors with a nearly constant phase over a wide range of angles, resulting in a rigid quadratic dispersion. Typical vertical microcavities are made of two distributed Bragg reflectors (DBRs), each consisting of multiple dielectric layers of alternating high and low refractive indices. Each layer in a DBR has an optical path length of $\lambda/4$, to maximize the reflectance at the design wavelength λ. As a result, the reflection phase of a DBR is integer times π at normal incidence and varies very slowly with increasing $k_\parallel$ [13]. For a $\lambda/2$ low-index cavity, $\phi_1(\omega, k_\parallel) \approx \phi_2(\omega, k_\parallel) \approx \pi$ and $m = 0$. Using $k_{c\perp} = \sqrt{(n_c\omega/c)^2 - k_\parallel^2}$, for small $k_\parallel$, we obtain a quadratic dispersion,

$$\omega(k_\parallel) \approx \omega_0\left[1 + \frac{k_\parallel^2}{2(n_c\omega_0/c)^2}\right]. \tag{2}$$

Here $\omega_0 = \omega(k_\parallel = 0)$ and n_c is the refraction index of the cavity. For an AlAs cavity, $k_\parallel^2/(n_c\omega_0/c)^2 < 0.1$ is satisfied for an incidence angle up to $\theta_0 = 44°$ in vacuum. The curvature of the quadratic dispersion is determined by n_c and ω_0, with no additional tuning available.

In contrast, we use an SWG as the cavity mirror [14,15], which has many tunable parameters, enabling strong angular dependencies of the reflection phase and, thus, dispersion engineering. A schematic of an SWG-DBR cavity we propose for dispersion engineering is shown in Fig. 1(a). The top mirror consists of an SWG suspended in air. The SWG has three grating parameters: its thickness (t_g), period (Λ), and duty cycle (η), as shown in Fig. 1(b). These parameters, together with the thickness of the air gap beneath the SWG, can provide flexibilities in cavity design that are unavailable in DBR-DBR cavities. For example, polarization selectivity and resonance tuning have been demonstrated in vertical cavity surface-emitting lasers (VCSELs) using SWGs as top mirrors [16–20]. Recently, strong-coupling and exciton-polariton lasing have been demonstrated in a zero-dimensional SWG-DBR cavity [21,22]. These works on vertical SWG cavities have mainly focused on modes with nearly zero in-plane momentum. Here we explore the angular dependence of the reflection phase of the SWG to demonstrate the unique capability of dispersion engineering in an SWG-based cavity.

Unlike from a DBR, reflection from the periodic SWG structure is produced by the scattering between the lateral modes inside the SWG and Floquet-form diffraction modes outside [23–25]. The lateral modes of an SWG are therefore the key to understanding its reflection phase. We adopt the waveguide-array (WGA) modes formulation, which was introduced in [25] to explain intuitively the high reflectance of the SWG at normal incidence. Below we generalize the work in [25] and derive the WGA modes in SWGs of arbitrary thickness in the general case of oblique incidence. We will show that, due to symmetry properties of the grating, the dispersion of the WGA modes could shift considerably with the incidence angle, leading to large changes in the reflection phase.

We treat the SWG as a waveguide array with the z axis as the propagation direction, as shown in Fig. 1(b). It is periodic in the x direction and translationally invariant in the y direction. We focus the discussion on the case of an incident plane wave propagating in the x-z plane with an oblique angle θ_0 from the z direction. For a WGA mode with a TM polarization as labeled in Fig. 1(b), the lateral mode profile $H(x)$ and propagation constant β are determined by the eigenvalue equation

$$\left[\frac{\partial^2}{\partial x^2} + n^2(x)\frac{\omega^2}{c^2}\right]H(x) = \beta^2 H(x) \tag{3}$$

where $n(x)$ is the refractive index. Because of the periodicity of $n(x)$, the eigenmode can be expressed in the form of Bloch waves,

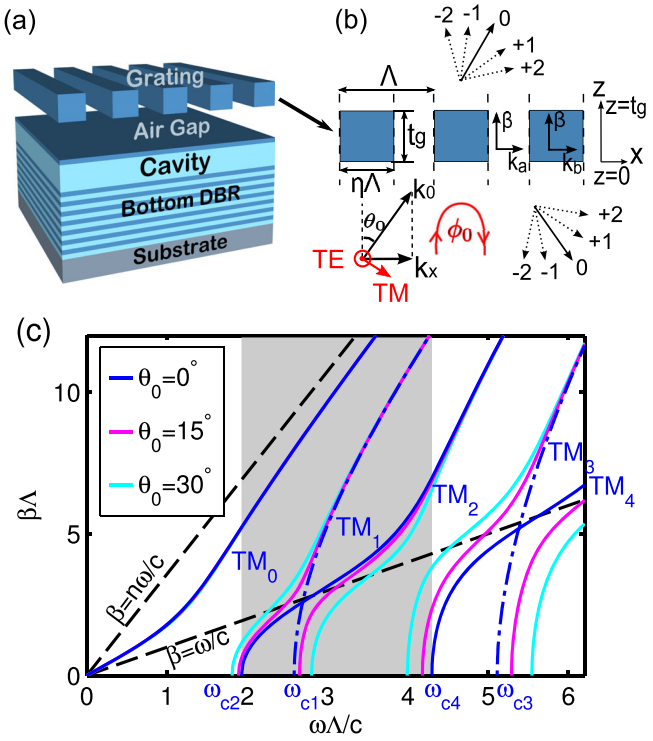

FIG. 1 (color online). (a) Schematic of an SWG-DBR hybrid vertical cavity. The SWG followed by an air gap and one high-index DBR layer comprise the top mirror. We use $Al_{0.15}Ga_{0.85}As$ (refractive index $n_r = 3.58$) for the grating bars and high-index DBR layers, and AlAs ($n_r = 3.02$) for the low-index DBR and cavity layers. (b) Cross section of an SWG and the wave vectors inside and outside the SWG. The SWG is treated as a WGA between input plane $z = 0$ and output plane $z = t_g$. The light outside the WGA is the superposition of diffraction modes, with only the zero-order mode propagating for an SWG and the higher-order ones evanescent. ϕ_0 is the reflection phase of the zero-order wave. (c) The $\beta - \omega$ dispersions of the transverse-magnetic (TM) WGA modes in an SWG with a duty cycle $\eta = 65\%$, for incidence angles of 0° (blue line), 15° (pink), and 30° (cyan). Dash-dotted lines mark modes that cannot be excited. The zeroth WGA modes at different angles almost overlap with the TM_0 mode. The higher modes shift with the incidence angle, leading to large changes in the reflection phase. The gray shade marks the dual-mode regime at normal incidence. The black dashed lines are the dispersions of light in homogeneous air and grating-bar dielectric medium.

$$H(x) = e^{ik_x x}u_n(x),$$

where $e^{ik_x x}$ is the Bloch phase factor, k_x is the in-plane wave number of the incident wave ($k_x = \omega/c \sin\theta_0$), $u_n(x)$ is a periodic function, and the subscript n denotes the discrete mode number. Given ω and θ_0, we can solve for the eigenvalues β_n^2 and obtain the $\omega - \beta$ dispersion of the WGA modes through [26]

$$2n_b^2 k_a k_b(\cos k_a a \cos k_b b - \cos k_x \Lambda) - (n_b^4 k_a^2 + k_b^2)\sin k_a a \sin k_b b = 0. \tag{4}$$

Here n_b is the refractive index of the grating bar, a and b are the widths of the air and bar regions, and $k_{a,b}$ is the transverse wave number in the air or bar region, determined by $k_{a,b} = \sqrt{(n_{a,b}\omega/c)^2 - \beta^2}$. An example of a WGA mode dispersion is shown in Fig. 1(c).

In the case of normal incidence (blue lines), the incident wave matches the reflection symmetry of the grating about the center of the grating bars. Correspondingly, $TM_{0,2,4,\ldots}$. modes have the same symmetry and thus can be excited, while the $TM_{1,3,5,\ldots}$. modes have the odd symmetry and thus cannot be excited.

In the case of oblique-angle incidence, the incident plane waves no longer have the reflection symmetry, and, thus, the odd-order modes can also be excited. Avoided crossings between the odd-order and even-order modes lead to significant shift of the mode dispersions, as illustrated in Fig. 1(c).

Reflection from an SWG with a finite thickness t_g can be understood as resulting from the interference of WGA modes reflected from both the top and bottom SWG-air interfaces. For a given WGA, for example, the WGA used in Fig. 1(c), we can visualize the dependence of the reflection on t_g using t_g-ω maps of the reflectance and reflection phase, as shown in Fig. 2.

At normal incidence, for each of the WGA modes in Fig. 1(c), the SWG forms a Fabry-Perot resonator when the approximated round-trip phase condition $\beta t_g = m\pi$ is satisfied, where m is an integer [27]. We mark the corresponding $t_g - \omega$ values in Figs. 2(a)–2(b) with white dashed and dash-dotted lines for the TM_0 and TM_2 modes, respectively. The reflectance is nearly zero around these lines and the reflection phase changes by π across the lines, which are signatures of Fabry-Perot resonances. Naturally, high-reflectance regions exist only between these lines, when two WGA modes coexist and produce nearly perfect destructive interference at the output plane of SWG [25,28].

At oblique angles, the appearance of the odd-order WGA modes leads to large shifts of the WGA modes, which manifests as large shifts of the reflectance and phase patterns on the $t_g - \omega$ maps. An example is shown in Fig. 2(c)–2(d) for $\theta_0 = 30°$. Consistent with the $\beta - \omega$ diagram [Fig. 1(c)], the Fabry-Perot resonance lines originated from the TM_0 mode barely move, while those from the TM_2 mode move toward lower frequencies. The high-reflectance regions, as well as the phase in these regions, move with those "grid lines." For a certain SWG in the high-reflectance region, for example, the point marked by a white star in Fig. 2, the reflection phase could become very different at oblique incidence angles.

Now we show a few examples of dispersion engineering using SWGs. Two examples of SWGs are shown in Fig. 3(a), whose reflection phases change significantly with the incidence angle but in opposite ways. The reflection phase of SWG1 increases by 0.35π from $\theta_0 = 0°$ to 22°, while that of SWG2 decreases by 0.25π. In comparison, the reflectance phase of the DBR mirror changes by 0.03π.

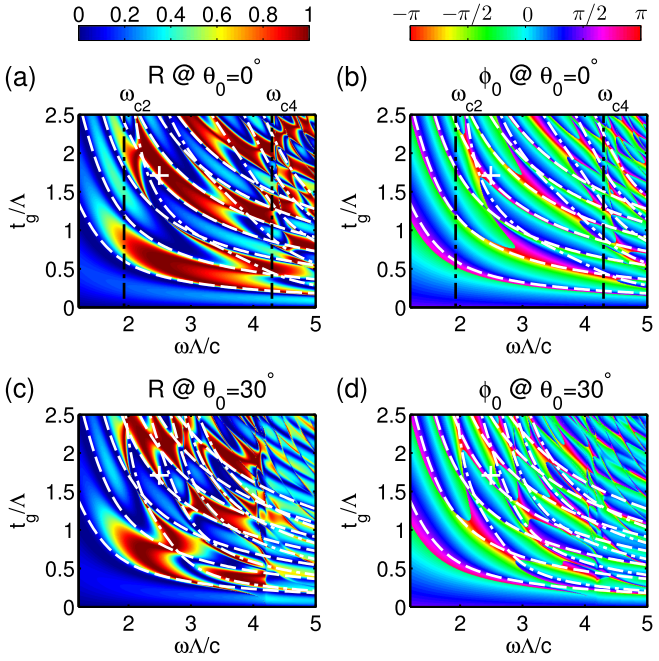

FIG. 2 (color online). $t_g - \omega$ maps of the reflectance [(a) and (c)] and reflection phase [(b) and (d)] of an SWG with $\eta = 65\%$ for the TM polarization, under normal incidence [(a) and (b)] and $\theta_0 = 30°$ oblique incidence [(b) and (d)]. The black dash-dotted lines in (a) and (b) show the dual-mode regime defined by ω_{c2} and ω_{c4} obtained in Fig. 1(c). The dispersions of the dual WGA modes are plotted as the two sets of white dashed and dash-dotted lines in all four figures, using the approximated Fabry-Perot resonance condition of $\beta t_g = \pi$. These lines overlap well with the zero-reflectance (blue) stripes in (a) and (c). Broadband high-reflectance regions (red) can be found between those lines. Each point on the figure corresponds to one SWG design. An example is marked by the white + symbol, which has a phase shift of $\sim 0.4\pi$ over 30° while maintaining high reflectance (> 0.995). The large phase shift is caused by the large WGA-mode shift, as seen by comparing the dash-dotted white lines in (b) and (d).

When using SWG1 and SWG2 as the top mirrors of SWG-DBR cavities, the cavity dispersion also changes drastically from that of the DBR-DBR cavity. As shown in Fig. 3(b), the SWG1-DBR cavity has a much steeper dispersion. Its resonance energy increases to 20 meV above the DBR-DBR cavity's resonance at $\theta_0 = 20°$. The SWG2-DBR cavity, on the other hand, features a nearly flat dispersion up to $k_{\|} \sim 2\ \mu m^{-1}$, or $\theta_0 \sim 15°$.

If the bottom DBR is also replaced by an SWG [29], the round-trip phase change is doubled, providing more tuning of the cavity dispersion. Figure 3(c) shows that the dispersion of the SWG1-SWG1 cavity becomes even steeper, while the dispersion of SWG2-SWG2 cavity reverses the sign and becomes negative. Moreover, dispersions of exotic shapes can also be created, such as the one shown in Fig. 3(d), which features a double-well shape.

These special dispersions are also robust against small variations in the grating parameters and, thus, are

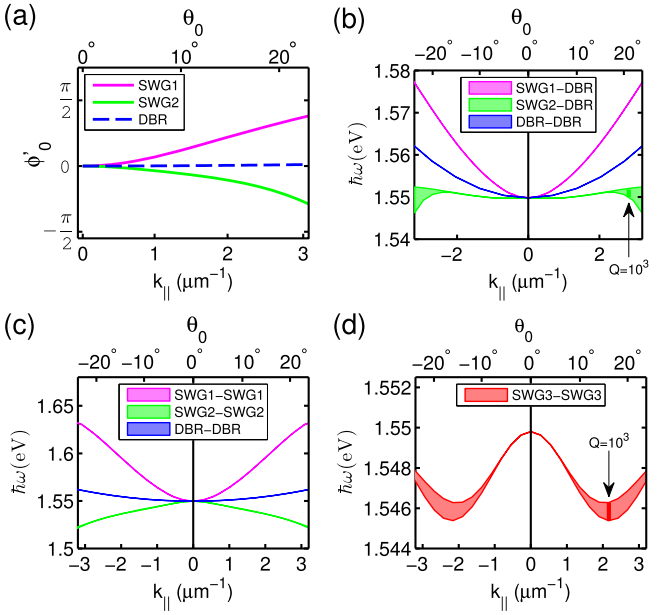

FIG. 3 (color online). (a) Comparison of the angular dependence of the reflection phase of two SWGs with a DBR. ϕ_0' is the shifted reflection phase that starts with zero at normal incidence. (b) Energy dispersions of cavities with the SWGs and DBR as in (a) as the top mirror and a bottom DBR with 30 $\lambda/2$ pairs. The linewidths of the cavity resonances $\delta(\hbar\omega)$ are shown as the shades, to indicate the quality factors of the cavities $Q = \omega/\delta\omega$. The linewidth corresponding to $Q = 10^3$ is marked. The curvature of dispersion is proportional to the effective mass defined as $m^* \equiv \hbar(d^2\omega/dk^2)^{-1}$. We obtain at $k_\parallel \sim 0$ an effective mass $m^* \approx 3 \times 10^{-5} m_e$ for the DBR-DBR cavity, where m_e is the mass of an electron. In comparison, $m^* \approx 1 \times 10^{-5} m_e$ for SWG1-DBR, $m^* \approx -20 \times 10^{-5} m_e$ for SWG2-DBR. (c) Energy dispersions of SWG1-SWG1 and SWG2-SWG2 cavities compared to the DBR-DBR cavity, showing more substantial tuning of the dispersion than in SWG-DBR cavities. At $k_\parallel \sim 0$, we obtain $m^* \approx 0.3 \times 10^{-5} m_e$ for SWG1-SWG1, and $m^* \approx -0.6 \times 10^{-5} m_e$ for the SWG2-SWG2 cavity. (d) A double-well-shaped dispersion for TM-polarized light in the SWG3-SWG3 cavity. The materials used in the cavities are given in Sec. 2. All dimensions are scaled to give a resonance of 1.55 eV at normal incidence. The structural parameters are as follows: SWG1: $\Lambda = 539$ nm, $t_g = 350$ nm, $\eta = 0.31$, transverse electric polarization; SWG2: $\Lambda = 328$ nm, $t_g = 557$ nm, $\eta = 0.65$, TM polarization; SWG3: $\Lambda = 300$ nm, $t_g = 584$ nm, $\eta = 0.62$, TM polarization.

achievable with present fabrication technologies [32]. We consider variations in the thickness t_g by ± 5 nm due to errors in the epitaxial growth, and in the period Λ and bar width $\eta\Lambda$ by ± 2 nm due to the resolution of electron-beam lithography. For the SWG1-DBR cavity, its effective mass m^* changes by less than 13%; hence, the steep dispersion is well maintained. For the SWG2-DBR cavity, designed to have a flat dispersion, the effective mass is reduced by fourfold with a 2-nm increase in $\eta\Lambda$, but remains heavier than that of the DBR-DBR cavity. The variations due to the e-beam resolution can be further reduced by using the e-beam dose matrix to create SWGs with slightly varying Λ and η. For the SWG3-SWG3 cavity, its resonance changes by less than 0.3 meV, much less than the well depth of $\sim$4 meV; hence, the double-well shape is robust against the fabrication errors.

Since dispersion is a fundamental property of a photonic system, such tunability of the dispersion may enable many novel applications. For example, it may be used to control the propagation of light, since the group velocity of the photon is proportional to $d\omega/dk$. A steeper or shallower dispersion leads to faster or slower propagation of light. A nearly flat dispersion may enable slow light and storage of light in the cavity. Changing the dispersion also changes the spontaneous decay rate of excitations enclosed inside the cavity via Purcell enhancement or suppression [36]. The Purcell factor is proportional to the energy DOS of photons, which in turn depends on the effective mass $m^* \equiv \hbar^2(d^2E/dk^2)^{-1}$ of the cavity modes, or the curvature of the dispersion curve. A steep dispersion will suppress spontaneous emission, while a flat dispersion would lead to divergent DOS and a very high Purcell enhancement. The SWG2-DBR cavity, for example, has an effective mass $m^* \approx -20 \times 10^{-5} m_e$, more than six times heavier than the DBR-DBR cavity's effective mass of $m^* \approx 3 \times 10^{-5} m_e$. It thus may allow a Purcell enhancement of sixfold compared to a planar DBR-DBR cavity.

The proposed cavity structure can also be used in polariton systems to control the properties of polariton condensates and lasers [37,38], and to create novel many-body systems. Unique to the proposed cavity, it simultaneous allows lossless integration of active media in the cavity layer and a high cavity quality factor due to the high reflectance of the SWG. A zero-dimensional polariton laser was recently demonstrated in an SWG-DBR cavity [21] with a cavity quality factor of a few thousands. All the SWGs shown in Fig. 3 are optimized for high reflectance at normal incidence, giving cavity $Q > 10^4$. At oblique angles, their reflectance vary, but the cavity Q remains above 10^3 up to $\theta = \pm 20°$ [39]. Hence the strong-coupling regime should be readily reached when multiple quantum wells are placed at the antinodes of these high-Q cavities [40].

In the strong-coupling regime, the cavity dispersion is directly transcribed to the polariton dispersion [41]. Changing the effective mass of the polariton, independent of changing the exciton fraction in the polariton mode, would allow one to control the dynamics and condensate formation. Polariton systems with a lighter effective mass without reduced exciton fraction, such as in the SWG1-DBR cavity, may achieve a higher phase-space density at lower excitation densities. They may enable polariton lasers at an even lower threshold than that demonstrated in DBR-DBR cavities [43–46], and may facilitate the BEC-BCS crossover transition [47–49]. On the other hand, polaritons with a heavy effective mass without reduced photon

fraction, such as in the SWG2-DBR cavity, may allow rapid thermalization of polaritons while maintaining robust coherence. That may facilitate the formation of equilibrium quantum phases in polaritons. Tuning the polariton dispersion also tunes its group velocity, enabling, for example, faster polariton transport within its short lifetime, or slow light and slow polariton delay lines in optical and polaritonic circuits [50]. Finally, the flexibility to create dispersion of unusual symmetries may open a door to novel physics. The double-well dispersion in the SWG3-SWG3 cavity may show spontaneous symmetry breaking when particles relax from the metastable zero-k state to the two degenerated ground states. It may also allow the observation of the Josephson effect in momentum space [51] and may be extended to create systems with artificial magnetic fields and topological states [4,12].

In short, we showed how to utilize the large angular dependence of the reflection phase of SWGs to engineer the dispersion of a vertical cavity. The cavity can retain a high quality factor and is compatible with lossless integration of active media. The curvature of the dispersion of SWG-based cavities can be tuned by several orders of magnitude. Even flat, inversed, or double-well-shaped dispersions can be created. Such flexibility in dispersion engineering may benefit many research areas such as Purcell enhancement in 2D structures, polariton-based lasers and quantum circuits, and exotic quantum phases in polaritons.

Z. W., B. Z., and H. D. acknowledge the support by the National Science Foundation (NSF) under Grant No. DMR 1150593 and the Air Force Office of Scientific Research under Grant No. FA9550-12-1-0256. We thank Pavel Kwiecien for his open-source RCWA code used for calculations in this Letter. We thank Professor Ted Norris and Professor Kai Sun for helpful discussions. We thank Lei Zhang for help in initial calculations.

*Corresponding author.
dengh@umich.edu

[1] R. W. Boyd and D. J. Gauthier, Science **326**, 1074 (2009).
[2] S. Haroche and D. Kleppner, Phys. Today **42**, 24 (1989).
[3] Y.-J. Lin, K. Jimnez-Garca, and I. B. Spielman, Nature (London) **471**, 83 (2011).
[4] H. M. Price, T. Ozawa, and I. Carusotto, Phys. Rev. Lett. **113**, 190403 (2014).
[5] V. M. Shalaev, Nat. Photonics **1**, 41 (2007).
[6] Z. Jacob, J.-Y. Kim, G. V. Naik, A. Boltasseva, E. E. Narimanov, and V. M. Shalaev, Appl. Phys. B **100**, 215 (2010).
[7] M. A. Noginov, H. Li, Y. A. Barnakov, D. Dryden, G. Nataraj, G. Zhu, C. E. Bonner, M. Mayy, Z. Jacob, and E. E. Narimanov, Opt. Lett. **35**, 1863 (2010).
[8] H. N. S. Krishnamoorthy, Z. Jacob, E. Narimanov, I. Kretzschmar, and V. M. Menon, Science **336**, 205 (2012).
[9] T. F. Krauss, J. Phys. D **40**, 2666 (2007).
[10] T. Baba, Nat. Photonics **2**, 465 (2008).
[11] S. Noda, M. Fujita, and T. Asano, Nat. Photonics **1**, 449 (2007).
[12] J. Dalibard, F. Gerbier, G. Juzeliūnas, and P. Öhberg, Rev. Mod. Phys. **83**, 1523 (2011).
[13] See Supplemental Material at http://link.aps.org/supplemental/10.1103/PhysRevLett.114.073601 for comparison of the reflection phases of a DBR and an SWG.
[14] C. F. R. Mateus, S. Member, M. C. Y. Huang, Y. Deng, A. R. Neureuther, and C. J. Chang-Hasnain, IEEE Photonics Technol. Lett. **16**, 518 (2004).
[15] C. F. R. Mateus, S. Member, M. C. Y. Huang, L. Chen, C. J. Chang-Hasnain, and Y. Suzuki, IEEE Photonics Technol. Lett. **16**, 1676 (2004).
[16] S. J. Schablitsky, L. Zhuang, R. C. Shi, and S. Y. Chou, Appl. Phys. Lett. **69**, 7 (1996).
[17] M. C. Y. Huang, Y. Zhou, and C. J. Chang-Hasnain, Nat. Photonics **1**, 119 (2007).
[18] M. C. Y. Huang, Y. Zhou, and C. J. Chang-Hasnain, Nat. Photonics **2**, 180 (2008).
[19] V. Karagodsky, B. Pesala, C. Chase, W. Hofmann, F. Koyama, and C. J. Chang-Hasnain, Opt. Express **18**, 694 (2010).
[20] Y. Rao, C. Chase, and C. J. Chang-Hasnain, *22nd IEEE International Semiconductor Laser Conference* (ISLC, Kyoto2010), p. 11.
[21] B. Zhang, Z. Wang, S. Brodbeck, C. Schneider, M. Kamp, S. Höfling, and H. Deng, Light Sci. Appl. **3**, e135 (2014).
[22] J. Fischer, S. Brodbeck, B. Zhang, Z. Wang, L. Worschech, H. Deng, M. Kamp, C. Schneider, and S. Höfling, Appl. Phys. Lett. **104**, 091117 (2014).
[23] M. G. Moharam, E. B. Grann, D. A. Pommet, and T. K. Gaylord, J. Opt. Soc. Am. A **12**, 1068 (1995).
[24] R. Magnusson and M. Shokooh-Saremi, Opt. Express **16**, 3456 (2008).
[25] V. Karagodsky, F. G. Sedgwick, and C. J. Chang-Hasnain, Opt. Express **18**, 16973 (2010).
[26] See Supplemental Material at http://link.aps.org/supplemental/10.1103/PhysRevLett.114.073601 for the derivation of the dispersion of WGA modes.
[27] V. Karagodsky, C. Chase, and C. J. Chang-Hasnain, Opt. Lett. **36**, 1704 (2011).
[28] V. Karagodsky and C. J. Chang-Hasnain, Opt. Express **20**, 10888 (2012).
[29] For possible ways of fabricating the SWG-SWG cavity, refer to [17,30,31].
[30] C. Sciancalepore, B. Ben Bakir, C. Seassal, X. Letartre, J. Harduin, N. Olivier, J. Fedeli, and P. Viktorovitch, IEEE Photonics J. **4**, 399 (2012).
[31] K. Aoki, D. Guimard, M. Nishioka, M. Nomura, S. Iwamoto, and Y. Arakawa, Nat. Photonics **2**, 688 (2008).
[32] See Supplemental Material at http://link.aps.org/supplemental/10.1103/PhysRevLett.114.073601 for fabrication error tolerance analysis, which includes Refs. [33–35].
[33] N. Arjmandi, L. Lagae, and G. Borghs, J. Vac. Sci. Technol. B **27**, 1915 (2009).
[34] H. Duan, V. R. Manfrinato, J. K. W. Yang, D. Winston, B. M. Cord, and K. K. Berggren, J. Vac. Sci. Technol. B **28**, C6H11 (2010).
[35] V. R. Manfrinato, L. Zhang, D. Su, H. Duan, R. G. Hobbs, E. A. Stach, and K. K. Berggren, Nano Lett. **13**, 1555 (2013).

[36] E. M. Purcell, H. C. Torrey, and R. V. Pound, Phys. Rev. **69**, 37 (1946).
[37] H. Deng, H. Haug, and Y. Yamamoto, Rev. Mod. Phys. **82**, 1489 (2010).
[38] I. Carusotto and C. Ciuti, Rev. Mod. Phys. **85**, 299 (2013).
[39] See Supplemental Material at http://link.aps.org/supplemental/10.1103/PhysRevLett.114.073601 for the angular dependence of the quality factors of the SWG cavities.
[40] C. Weisbuch, M. Nishioka, A. Ishikawa, and Y. Arakawa, Phys. Rev. Lett. **69**, 3314 (1992).
[41] The effective mass of the lower polaritons (LPs) is given by $m_{\mathrm{LP}}^{-1} = |X|^2/m_{\mathrm{exc}} + |C|^2/m_{\mathrm{cav}}$, where the X and C are Hopfield coefficients representing the exciton and cavity photon fractions in a LP [42], and m_{exc} and m_{cav} are the effective masses of the exciton and cavity, respectively. Since $m_{\mathrm{exc}} \sim 10^4 m_{\mathrm{cav}}$, $m_{\mathrm{LP}} \approx m_{\mathrm{cav}}/|C|^2$. Tuning of the photon dispersion thus directly tunes the polariton dispersion.
[42] J. J. Hopfield and D. G. Thomas, Phys. Rev. **132**, 563 (1963).
[43] H. Deng, G. Weihs, D. Snoke, J. Bloch, and Y. Yamamoto, Proc. Natl. Acad. Sci. U.S.A. **100**, 15318 (2003).
[44] G. Christmann, R. Butte, E. Feltin, J.-F. Carlin, and N. Grandjean, Appl. Phys. Lett. **93**, 051102 (2008).
[45] S. Kena-Cohen and S. R. Forrest, Nat. Photonics **4**, 371 (2010).
[46] T.-C. Lu, Y.-Y. Lai, Y.-P. Lan, S.-W. Huang, J.-R. Chen, Y.-C. Wu, W.-F. Hsieh, and H. Deng, Opt. Express **20**, 5530 (2012).
[47] C. Comte and P. Nozières, J. Phys. (Orsay, Fr.) **43**, 1069 (1982).
[48] P. B. Littlewood, P. R. Eastham, J. M. J. Keeling, F. M. Marchetti, B. D. Simon, and M. H. Szymanska, J. Phys. Condens. Matter **16**, S3597 (2004).
[49] T. Byrnes, T. Horikiri, N. Ishida, and Y. Yamamoto, Phys. Rev. Lett. **105**, 186402 (2010).
[50] T. Liew, I. Shelykh, and G. Malpuech, Physica (Amsterdam) **43E**, 1543 (2011).
[51] R. E. Troncoso and l. S. Nez, Ann. Phys. (Amsterdam) **346**, 182 (2014).